NASA TECHNICAL MEMORANDUM 101527

A RE-EVALUATION OF FINITE-ELEMENT MODELS AND STRESS-INTENSITY FACTORS FOR SURFACE CRACKS EMANATING FROM STRESS CONCENTRATIONS

P.W.Tan, I.S. Raju,
K.N. Shivakumar, and J. C. Newman, Jr.

November 1988

National Aeronautics and
Space Administration

Langley Research Center
Hampton, Virginia 23665-5225

INTRODUCTION

Surface and corner cracks can occur in many structural components. These cracks can cause premature failure of landing gear of aircraft, spars, stiffeners, and other reinforcements. Accurate stress analyses of these crack components are needed for reliable prediction of crack-growth rates and fracture strengths.

Surface and corner cracks in plates have received considerable attention in the literature in the past sixteen years [1-20]. Various methods: finite-element method with singularity elements [3,4,8,10,12,13,17,19], finite-element method with displacement hybrid elements [5,6], alternating method [1,2,7,9], finite-element-alternating method [14,15,18,20], and boundary-integral equation method [11], were used to obtain stress-intensity factors for these cracked components. Stress-intensity factor equations were obtained by fitting empirical equations to the stress-intensity factors obtained from numerical analyses [16,17].

Surface and corner cracks at holes have received much less attention than surface cracks in plates. Smith and Kullgren [9], and Raju and Newman [12], analyzed corner cracks from a circular hole by the alternating method and the finite-element method (with singularity elements), respectively. Nishioka and Atluri [15,18] analyzed corner cracks from a circular hole and corner cracks in a lug by the finite-element-alternating method. The stress-intensity factors by all of the above mentioned methods agreed well with one another [12,15], except in the region where the crack intersected the hole boundary. In this region, the stress-intensity factors from Raju and Newman [12,16] showed a precipitous "drop-off". The stress-intensity factors calculated by other investigators (see refs. 12 and 15) did not show the large drop-off near the hole-crack intersection. Thus, the primary purpose of this paper is to investigate the

reasons for the large drop in the stress-intensity factors where a surface crack meets a hole or notch boundary. In this investigation, an evaluation of the previously developed finite-element models used by Raju and Newman [12,16] and of the methods used to determine the stress-intensity factors was performed.

The second purpose of this paper is to present stress-intensity factors for a semi-elliptical surface crack located at the center of a semi-circular edge notch in a finite thickness plate. This crack configuration has not been analyzed in the literature. The plates were subjected to remote tension loads and a wide range in configuration parameters were considered. The ratio of crack depth along the notch root to crack length away from the notch root (a/c) ranged from 0.4 to 2; the ratio of crack depth to plate thickness (a/t) ranged from 0.2 to 0.8; and the ratio of notch radius to plate thickness (r/t) ranged from 1 to 3. The r/t ratio of 3 was chosen because this particular configuration was tested in an AGARD study on short-crack growth behavior [21].

SYMBOLS

a	half-depth of surface crack along notch root
b	width of plate
c	length of surface crack from notch root
F_{sn}	stress-intensity boundary-correction factor
h	half-height of plate
K	stress-intensity factor (mode I)
Q	shape factor for elliptical crack
r	radius of the semi-circular notch or circular hole
S	remote uniform tensile stress
t	half-thickness of plate

x,y,z	Cartesian coordinate system
ν	Poisson's ratio
ϕ	parametric angle of ellipse

THREE-DIMENSIONAL FINITE-ELEMENT ANALYSIS

A three-dimensional finite-element analysis was used to calculate the mode I stress-intensity factor variations along the crack front for a surface crack emanating from the center of a semi-circular edge notch (or a circular hole) in a plate subjected to tensile loading, as shown in Figure 1. In these analyses, Poisson's ratio was assumed to be 0.3.

Due to symmetry, only one quarter of the specimen was modeled for the notch configuration. Symmetry conditions on the x = 0 plane were used to model the circular hole configuration. A typical model is shown in Figure 2. This model has 8 wedges on the crack plane and 4 layers on the hole. Six-noded pentahedral singularity elements were used along the crack front and eight-noded hexahedral elements were used elsewhere. The finite-element models were subjected to remote tensile loading on the y = h plane. Stress-intensity factors were calculated using a nodal-force method. Details of the formulation of these types of elements and the nodal-force method are given in References 8, 10 and 12. Details on the development of the finite-element models will be discussed later.

Stress-Intensity Factor

The remote tensile loads cause only mode I deformations. The mode I stress-intensity factor K for any location along the crack front was taken to be

$$K = S\,(\pi a/Q)^{1/2}\;F_{sn}\,(\,a/t,\;a/c,\;r/t,\;\phi\,) \qquad (1)$$

The half-height of the plate, h, and width, b, were chosen large enough to have a negligible effect on stress-intensity factors ($h/b \geq 2$ and $r/b \simeq 0.05$). Values of F_{sn}, the boundary-correction factor, were calculated along the crack front for various combinations of parameters (a/t, a/c, r/t and ϕ). The crack dimensions and parametric angle, ϕ , are defined in Figure 1. The shape factor for an ellipse, Q, is given by the square of the complete elliptic integral of the second kind. Empirical expressions for Q (taken from ref. 10) were

$$Q = 1 + 1.464\,(a/c)^{1.65} \quad \text{for } a/c \leq 1 \qquad (2a)$$

$$Q = 1 + 1.464\,(c/a)^{1.65} \quad \text{for } a/c > 1 \qquad (2b)$$

Evaluation of Finite-Element Models and Methods

Stress-intensity factor distributions in References 12 and 16 for surface and corner cracks at a hole showed a precipitous "drop-off" near the region where the crack meets the hole boundary. This drop-off was believed to have been caused by the "boundary-layer" effect. However, comparisons (see refs. 12 and 15) with other solutions in the literature showed that the stress-intensity factors calculated by other investigators did not exhibit this large drop-off near the boundary-layer region. Therefore, a study was carried out to determine whether this drop-off is an artifact of the modeling or is a real behavior. The models used in References 12 and 16 were re-examined. This examination revealed that the procedures used to generate the solids produced models with some "ill-shaped" elements in the region where the crack intersects the hole boundary. These ill-shaped elements were produced when the "wedge" region along the crack

plane was connected directly to the "layer" region to model the hole or notch. For r/t = 1, the elements in the region where the crack meets the hole boundary had aspect ratios (ratio of largest to smallest dimension) of about 150. The aspect ratio of these elements increased linearly as the r/t ratio increased, that is, for r/t = 3 the aspect ratio was 450!

The "ill-shaped" elements were defined as those elements that had aspect ratios greater than 100. These elements do not have any influence on the results if they are in regions of small stress gradients. However, they tend to produce a stiffer model if they are located in regions of large stress gradients. Because these elements were found in the region where the crack intersects the hole boundary, an investigation was undertaken to study the influence of these ill-shaped elements on the stress-intensity factor solutions. Three different finite-element models were developed and two different methods were used to extract the stress-intensity factors from the finite-element solutions.

Models.- Model A used finite-element patterns that were similar to those used in References 12 and 16 with the "ill-shaped" elements near the hole-crack intersection. Model B was a newly-developed finite-element model similar to Model A but without ill-shaped elements. Both Models A and B used a polar mesh and singularity elements around the crack front, as shown in Figure 2. Model C, on the other hand, used a rectangular mesh and non-singular elements around the crack front. Also, Model C did not have any ill-shaped elements near the hole-crack intersection. In Models B and C, the ill-shaped elements were avoided by not directly connecting the wedge region to the layer region near the hole-crack intersection. A small offset (less than 0.04r) was used before the layers were added to model the hole or notch configuration (see fig. 2). The x-coordinates

of the nodes in the "offset" region were adjusted so that they lie on the circular boundary.

Two different in-house (NASA Langley) computer programs, discussed in References 12 and 23, were used to analyze the various models. The different computer programs were used to verify the consistency of the results and to determine whether any undetected errors existed in the computer codes and analyses.

In Models A and B, pentahedron singularity elements were used all along the crack front and 8-noded hexahedron elements were used to model the rest of the solid. Furthermore, a 3x3x3 Gaussian integration scheme was used to form the element stiffness matrices. In Model C, non-singular 8-noded hexahedron elements were used everywhere to model the solid. A 2x2x2 Gaussian integration scheme and reduced integration for the shear terms [23] were used in conjunction with Model C. In contrast to Models A and B, where the models had a polar-mesh pattern around the crack front, Model C had a rectangular-mesh pattern around the crack front.

Methods.- Two methods for extracting stress-intensity factors from the solutions were also studied. The methods were the nodal-force method [8,10,12] and the virtual-crack-closure technique (VCCT) [23,24]. In the nodal-force method, the forces normal to the crack plane and ahead of the crack front were used to calculate the stress-intensity factors. This method does not require the assumption of either plane stress or plane strain to obtain the stress-intensity factor. The VCCT calculates the strain-energy release rate using the forces normal to the crack plane and ahead of the crack front and the relative displacements of the crack faces behind the crack front. The stress-intensity factor is then obtained from the calculated strain-energy release rate by assuming either plane-strain or plane-stress conditions. Plane-strain

conditions were used everywhere along the crack front except where the crack meets the notch surface (ϕ = 90°). At this location, plane-stress conditions were used. These types of assumptions along the crack front are widely used in the literature [4,11,13,23,24].

Comparison of stress-intensity factors.- Three specimen configurations with r/t = 1 or 3 were chosen in the evaluation study. All configurations had a semi-circular (a/c = 1) crack with an a/t ratio of 0.2. One configuration had a surface crack emanating from a circular hole (r/t = 1) while the other configurations had a surface crack emanating from a semi-circular edge notch (r/t = 1 and 3). All models had 14 wedges to model the crack plane and 10 layers to model the notch. Models A and B had about 15,000 degrees-of-freedom (dof) while Model C had about 18,000 dof.

Figure 3 presents the stress-intensity factor distributions along the crack front from Models A, B and C for a surface crack located at the center of a circular hole with r/t = 1. The results from Models B and C agreed well (within 1.5 percent) with each other all along the crack front. Model A, with the "ill-shaped" elements (circular symbols [16]), gave stress-intensity factors that were lower than the results from the other models. The discrepancy was quite large for ϕ > 60°. The results from Models B and C do not show the large drop-off exhibited by Model A.

The solid curve is an empirical equation for a surface crack at a circular hole that was based on previous finite-element results [16]. Comparison with the present finite-element results suggests that the equation is still accurate (within 5 percent) for this crack configuration although a slight modification would be necessary near the hole-crack intersection.

Figures 4 and 5 present stress-intensity factors for the same crack shape and size as shown in Figure 3 (a/c=1; a/t=0.2) but for a surface crack at a

semi-circular edge notch with r/t ratios of 1 and 3, respectively. The nodal-force results from models with and without ill-shaped elements (Models A and B, respectively) differed all along the crack front especially for the results with r/t = 3. Again, the largest discrepancies occurred for $\phi > 60^{\circ}$. However, the nodal-force results (Model B) were in good agreement with results from Model C using the VCCT. The maximum difference between these two sets of results was only about 2 percent.

Again, the solid curves in these figures show stress-intensity factors calculated from an empirical equation [25]. This equation was previously fitted to finite-element results for a surface crack at a hole [16] but adjusted for the stress concentration differences between a hole and a notch. Comparison with the present finite-element results suggests that the equation is still accurate for this crack configuration although a slight modification would, again, be necessary near the hole-crack intersection (maximum difference at this location was about 5 percent). However, for r/t = 3, the equation consistently underestimated the stress-intensity factors (5 to 10 percent). A reason for the lower estimates is probably because the equation was extrapolated to r/t values beyond those used in fitting the equation ($0.5 \leq r/t \leq 2$). Thus, a modification to the equations is required for crack configurations with the r/t ratios greater than 2.

Discussion.- Recall that the nodal-force method was used to extract the stress-intensity factors from the models with and without the ill-shaped elements (Model A and B, respectively). On the other hand, the VCCT was used in conjunction with Model C. All models without the ill-shaped elements gave nearly the same stress-intensity factors all along the crack front. This suggests that the two methods of extracting stress-intensity factors are

reliable, provided that the models are well behaved. The models with the "ill-shaped" elements tended to make the model too stiff and, hence, gave lower stress-intensity factors than models without these elements. Therefore, improved finite-element models that were similar to those used in References 12 and 16 but did not contain any ill-shaped elements were developed for a wide range in configuration parameters. These new models, in conjunction with the nodal-force method, were used to analyze a surface crack at a semi-circular edge notch herein. These models had about 15,000 dof. The results obtained with these models are discussed in the following section.

STRESS-INTENSITY FACTOR SOLUTIONS FOR SURFACE CRACK AT SEMI-CIRCULAR EDGE NOTCH

A surface crack emanating from a semi-circular edge notch in a plate subjected to remote tensile loading was considered herein. A wide range in crack sizes (a/t), crack shapes (a/c) and notch sizes (r/t) were analyzed. The ranges in crack and notch parameters were:

$a/t = 0.2, 0.5,$ and 0.8

$a/c = 0.4, 1,$ and 2

$r/t = 1, 2,$ and 3

These particular crack configurations were chosen to cover the range of crack shapes and sizes that have been observed to grow in experiments. Note that the $r/t = 3$ configuration corresponds to a specimen used in an AGARD study on short cracks (see refs. 21 or 25). For each combination of parameters, stress-intensity factors were obtained all along the crack front.

The normalized stress-intensity factors obtained with the three-dimensional finite-element analyses are presented in Tables 1-3. Typical results are shown and discussed herein.

The normalized stress-intensity factor variations all along the crack front for the AGARD short-crack specimen with r/t = 3 are shown in Figures 6 and 7 for various crack shapes (a/c = 0.4 and 1, respectively). In these figures, the inserts show part of the crack plane with the relative size of the notch, half-thickness of the plate, and the various crack shapes and sizes considered. For both crack shapes, the maximum normalized stress-intensity factors occurred near the intersection of the crack front and the notch boundary (ϕ = 90°). This trend is expected because the crack front lies in a region that is influenced by the notch. Hence, surface cracks would be expected to grow more along the bore of the notch than away from the notch and approach an a/c ratio greater than unity. Experiments on surface cracks at notches [21,25] tend to support this observation.

Figure 8 shows the normalized stress-intensity factor variations along the crack front for a semi-elliptical surface crack with an a/c ratio of 2 and r/t = 1. In this case, the normalized stress-intensity factors are largest at the maximum crack length from the notch root (ϕ = 0°). For deep cracks (a/t = 0.8), the normalized stress-intensity factors are nearly constant all along the crack front.

The variation of normalized stress-intensity factors all along the crack front for various r/t ratios with a/c = 0.4 and a/t = 0.8 is shown in Figure 9. As expected, larger values of notch radii (higher r/t ratios) gave higher values of normalized stress-intensity factors for the same crack shape and size. This trend is expected because the crack surfaces are subjected to a higher normal

stress component for the larger r/t values. Similar trends were observed for all crack shapes and sizes analyzed and, hence, the results are not shown.

Figures 10 and 11 present the normalized stress-intensity factors at two locations along the crack front as a function of a/t for two different crack configurations. The stress-intensity factors at $\phi = 0^\circ$ and near the end of the other axis ($\phi = 80^\circ$) are presented. The 80° location was selected to avoid the boundary-layer region. Finite-element results were obtained for a/t ratios of 0.2, 0.5 and 0.8. The limiting solutions for a surface crack at a notch as a/t approaches zero were estimated from stress-intensity factor equations for a surface crack in a plate [16] and a stress concentration factor of 3.17 [25].

The normalized stress-intensity factors at $\phi = 0^\circ$ and 80° are shown in Figure 12 as a function of notch size (r/t) for an a/c ratio of 0.4. The results for the shallow crack (a/t = 0.2) are shown as solid curves, whereas the results for a deep crack (a/t = 0.8) are shown as dashed curves. These figures show that larger size notches (higher r/t ratios) tend to give higher normalized stress-intensity factors at both ends of the crack.

CONCLUDING REMARKS

A re-evaluation of the finite-element models and methods used to extract stress-intensity factors from finite-element solutions for surface cracks at stress concentrations was performed. Previous finite-element models used by Raju and Newman for surface and corner cracks at holes were shown to have "ill-shaped" elements at the intersection of the hole and crack boundaries. These ill-shaped elements tended to make the models too stiff and, hence, gave lower stress-intensity factors near the hole-crack intersection than models without

these elements. The improved models employed 8-noded elements and stress-intensity factors were calculated by both the nodal-force and virtual-crack-closure methods. Both methods and different models, without the ill-shaped elements, gave essentially the same results.

Comparisons made between the previously developed stress-intensity factor equations and the results from the improved models agreed well (within 5 percent) for configurations with notch-radii-to-plate-thickness (r/t) ratios less than 2. Larger discrepancies were shown for an r/t ratio of 3. Here, the stress-intensity factor equations gave results that were 5 to 10 percent lower than the results from the improved models for a semi-elliptical surface crack at a semi-circular edge notch.

Stress-intensity factors for semi-elliptical surface cracks emanating from from the center of a semi-circular edge notch in a plate subjected to remote tensile loading were obtained by three-dimensional finite-element analyses. A wide range of crack shapes, crack sizes, and notch-radius-to-plate-thickness ratios were considered. The range of crack sizes, defined by crack-depth-to-plate-thickness (a/t), considered was 0.2 to 0.8. The range of crack shapes, defined by the ratio of crack length along the notch to the crack length away from the notch root (a/c), considered was 0.4 to 2. The range of notch sizes, defined by the notch-radius-to-plate-thickness (r/t), considered was 1 to 3. The configuration with r/t = 3 was chosen because this is the configuration that was tested in an AGARD cooperative test program on growth of short cracks at notches.

REFERENCES

[1] Shah, R. C., and Kobayashi, A. S., "On the Surface Flaw Problem," In the Surface Crack: Physical Problems and Computational Solutions, J. L. Swedlow (Ed), ASME, American Society of Mechanical Engineers, 1972, pp. 79-142.

[2] Smith, F. W., "The Elastic Analysis of the Part-Circular Surface Flaw Problem by the Alternating Method," In the Surface Crack: Physical Problems and Computational Solutions, J. L. Swedlow (Ed), ASME, American Society of Mechanical Engineers, 1972, pp. 125-152.

[3] Tracey, D. M., "3D Elastic Singularity Element for Evaluation of K Along an Arbitrary Crack Front," Int. J. of Fracture, Vol. 9, 1973, pp. 340-343.

[4] Tracey, D. M., "Finite Element for Three-dimensional Elastic Crack Analysis", Nuclear Engineering and Design, Vol.26, 1974.

[5] Atluri, S. N., and Kathiresan, K., "An Assumed Displacement Hybrid Finite Element Model for Three-dimensional Linear Elastic Fracture Mechanics Analysis", Proc. 12th Annual Meeting of the Soc. Engr. Science, University of Texas, Austin, Texas, 1975.

[6] Kathiresan, K., "Three-dimensional Linear Elastic Fracture Mechanics Analysis by a Displacement Hybrid Finite Element Model," Ph. D. Thesis, Georgia Institute of Technology, 1976.

[7] Kobayashi, A. S. and Enetanya, A. N., "Stress Intensity Factor of a Corner Crack," Mechanics of Crack Growth, ASTM STP 590, American Society for Testing and Materials, 1976, pp. 477-495.

[8] Raju, I. S. and Newman, J. C., Jr., "Improved Stress-Intensity Factors for Semi-Elliptical Surface Cracks in Finite-Thickness Plates," NASA TM X-72825, 1977.

[9] Smith, F. W., and Kullgren, T. E., "Theoretical and Experimental Analysis of Surface Cracks Emanating from Fastener Holes", AFFDL-TR-76-104, Air Force Flight Dynamics Laboratory, 1977.

[10] Raju, I. S. and Newman, J. C., Jr., "Stress-Intensity Factors for a Wide Range of Semi-Elliptical Surface Cracks in Finite-Thickness Plates," Engineering Fracture Mechanics, Vol. 11, No. 4, 1979,pp. 817-829.

[11] Heliot, J., Labbens, R. C., and Pellissier-Tanon, A., "Semi-elliptical Surface Cracks Subjected to Stress Gradients", in Fracture Mechanics, C. W. Smith (Ed), ASTM STP 677, American Society for Testing of Materials, 1979, pp. 341-364.

[12] Raju, I. S., and Newman, J. C., Jr., "Stress-intensity Factors for Two Symmetric Corner Cracks," in Fracture Mechanics, ASTM STP 677, C. W. Smith (Ed), American Society of Testing and Materials, 1979, pp. 411-430.

[13] Pickard, A. C., "Stress-Intensity Factors for Cracks with Circular and Elliptic Crack Fronts - Determined by 3D Finite Element Methods," PNR-90035, Rolls-Royce Limited, May 1980.

[14] Nishioka, T., and Atluri, S. N., "Analytical Solution for Embedded Elliptical Cracks, and Finite Element-Alternating Method for Elliptical Surface Cracks, Subjected to Arbitrary Loadings," Engineering Fracture Mechanics, Vol. 17, 1983, pp 247-268.

[15] Nishioka, T., and Atluri, S. N., "An Alternating Method for Analysis of Surface Flawed Aircraft Structural Components", AIAA Jnl., Vol. 21, 1983, pp. 749-757.

[16] Newman, J. C., Jr. and Raju, I. S., "Stress-Intensity Factor Equations for Cracks in Three-Dimensional Finite Bodies," Fracture Mechanics: Fourteenth Symposium - Volume I: Theory and Analysis, ASTM STP 791, J. C. Lewis and G. Sines (Eds), American Society for Testing and Materials, 1983, pp. I-238 - I-265.

[17] Newman, J. C., Jr. and Raju, I. S., "Stress-Intensity Factor Equations for Cracks in Three-Dimensional Finite Bodies Subjected to Tension and Bending Loads," NASA TM-85793, April 1984.

[18] Atluri, S. N., and Nishioka, T., "Computational Methods for Three-dimensional Problems of Fracture", Chapter 7, In Computational Methods in Mechanics of Fracture, S. N. Atluri (Ed), North Holland, 1986, pp. 230-287.

[19] Raju, I. S. and Newman, J. C., Jr., "Finite-Element Analysis of Corner Cracks in Rectangular Bars," NASA TM-89070, 1987.

[20] Raju, I. S., Atluri, S. N., and Newman, J. C., Jr. "Stress-Intensity Factors for Small Surface and Corner Cracks in Plates," Paper Presented at the 20th National Symposium on Fracture Mechanics, Lehigh University, Bethlehem, Pa, June 23-25, 1987.

[21] Newman, J. C., Jr., and Edwards, P. R., "Short-Crack Growth Behaviour in an Aluminum Alloy - An AGARD Cooperative Test Programme," AGARD Report No. 732, 1988.

[22] Chermahini, R. G., Shivakumar, K. N., and Newman, J. C., Jr., "Three-Dimensional Finite-element Simulation of Fatigue-Crack Growth Closure," in Mechanics of Fatigue Crack Closure, J. C. Newman, Jr., and W. Elber (Eds), ASTM STP 982, Philadelphia, PA., 1988.

[23] Raju, I. S., Shivakumar, K. N., and Crews, J. H., Jr., "Three-Dimensional Elastic Analysis of a Composite Double Cantilever Beam Specimen," AIAA-87-0864, AIAA/ASME/ASCE/AHS, 27th Structures, Structural Dynamics, and Materials Conference, Monteray, CA., April 6-8, 1987.

[24] Shivakumar, K. N., Tan, P. W., and Newman, J. C., Jr., "A Virtual Crack-Closure Technique For Calculating Stress-Intensity Factors For Cracked Three Dimensional Bodies," International Journal of Fracture, Vol. 36, pp. R43 - R50, 1988.

[25] Swain, M. H. and Newman, J. C., Jr., "On the Use of Marker Loads and Replicas for Measuring Growth Rates for Small Cracks," in Fatigue Crack Topography, AGARD-CP-376, 1984, pp. 12.1-12.17.

Table 1. Boundary-correction factors, F_{sn}, for semi-elliptical surface crack emanating from the center of a semi-circular notch in a plate under tension. ($r/t=1$; $F_{sn} = K/[S(\pi a/Q)^{1/2}]$)

		a/t		
a/c	ϕ(deg)	0.2	0.5	0.8
0.4	0.0	1.113	0.869	0.833
	22.5	1.284	0.997	0.967
	45.0	1.678	1.296	1.274
	67.5	2.190	1.733	1.774
	78.8	2.567	2.129	2.232
	84.9	2.809	2.445	2.631
	88.0	2.938	2.655	2.951
	90.0	2.727	2.548	2.944
1	0.0	2.402	1.865	1.697
	22.5	2.442	1.904	1.716
	45.0	2.574	2.046	1.841
	67.5	2.826	2.355	2.211
	78.8	3.043	2.646	2.599
	84.9	3.192	2.858	2.898
	88.0	3.263	2.975	3.089
	90.0	2.858	2.656	2.826
2	0.0	1.988	1.545	1.299
	22.5	1.942	1.513	1.245
	45.0	1.831	1.453	1.173
	67.5	1.741	1.456	1.294
	78.8	1.719	1.491	1.409
	84.9	1.748	1.546	1.504
	88.0	1.781	1.590	1.566
	90.0	1.632	1.467	1.431

Table 2. Boundary-correction factors, F_{sn}, for semi-elliptical surface crack emanating from the center of a semi-circular notch in a plate under tension. ($r/t=2$; $F_{sn} = K/[S(\pi a/Q)^{1/2}]$)

a/c	ϕ(deg)	a/t = 0.2	a/t = 0.5	a/t = 0.8
0.4	0.0	1.405	1.081	0.989
	22.5	1.613	1.245	1.156
	45.0	2.070	1.634	1.553
	67.5	2.596	2.174	2.207
	78.8	2.943	2.595	2.764
	84.9	3.151	2.880	3.182
	88.0	3.252	3.044	3.469
	90.0	2.982	2.844	3.347
1	0.0	2.789	2.316	2.128
	22.5	2.822	2.357	2.152
	45.0	2.929	2.497	2.303
	67.5	3.138	2.780	2.715
	78.8	3.323	3.028	3.105
	84.9	3.454	3.201	3.378
	88.0	3.509	3.285	3.533
	90.0	3.052	2.885	3.161
2	0.0	2.309	1.832	1.595
	22.5	2.247	1.786	1.523
	45.0	2.098	1.683	1.413
	67.5	1.975	1.627	1.506
	78.8	1.945	1.624	1.594
	84.9	1.978	1.662	1.670
	88.0	2.015	1.697	1.720
	90.0	1.847	1.554	1.554

Table 3. Boundary-correction factors, F_{sn}, for semi-elliptical surface crack emanating from the center of a semi-circular notch in a plate under tension. ($r/t=3$; $F_{sn} = K/[S(\pi a/Q)^{1/2}]$)

a/c	ϕ(deg)	a/t = 0.2	a/t = 0.5	a/t = 0.8
0.4	0.0	1.603	1.253	1.131
	22.5	1.831	1.442	1.325
	45.0	2.318	1.882	1.788
	67.5	2.839	2.460	2.534
	78.8	3.167	2.878	3.135
	84.9	3.361	3.145	3.559
	88.0	3.452	3.290	3.834
	90.0	3.151	3.044	3.655
1	0.0	3.017	2.592	2.429
	22.5	3.045	2.630	2.454
	45.0	3.138	2.761	2.610
	67.5	3.328	3.022	3.032
	78.8	3.503	3.251	3.421
	84.9	3.629	3.411	3.685
	88.0	3.679	3.482	3.829
	90.0	3.192	3.040	3.398
2	0.0	2.368	2.000	1.777
	22.5	2.323	1.945	1.693
	45.0	2.212	1.818	1.559
	67.5	2.121	1.733	1.635
	78.8	2.087	1.715	1.713
	84.9	2.111	1.746	1.783
	88.0	2.142	1.779	1.830
	90.0	1.958	1.625	1.646

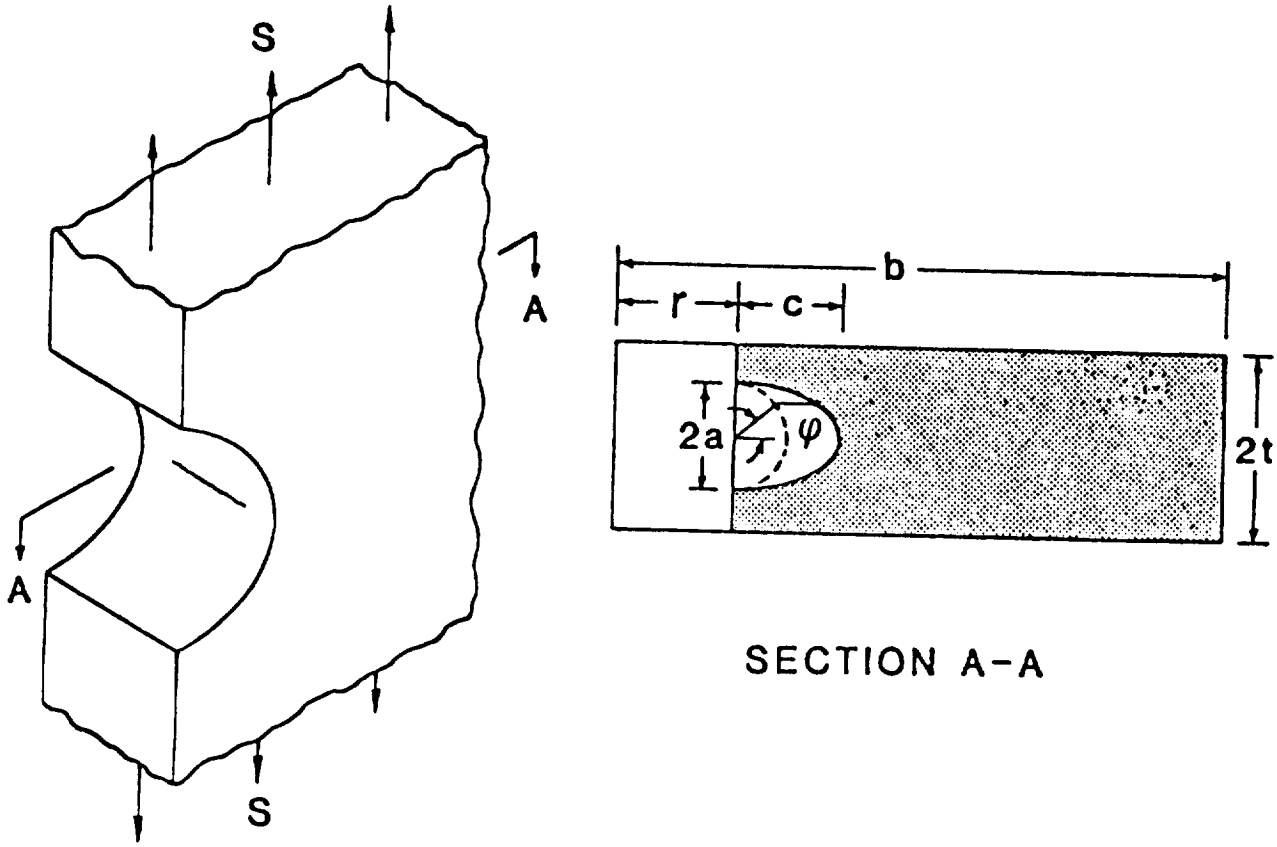

Figure 1.- Specimen configuration and loading.

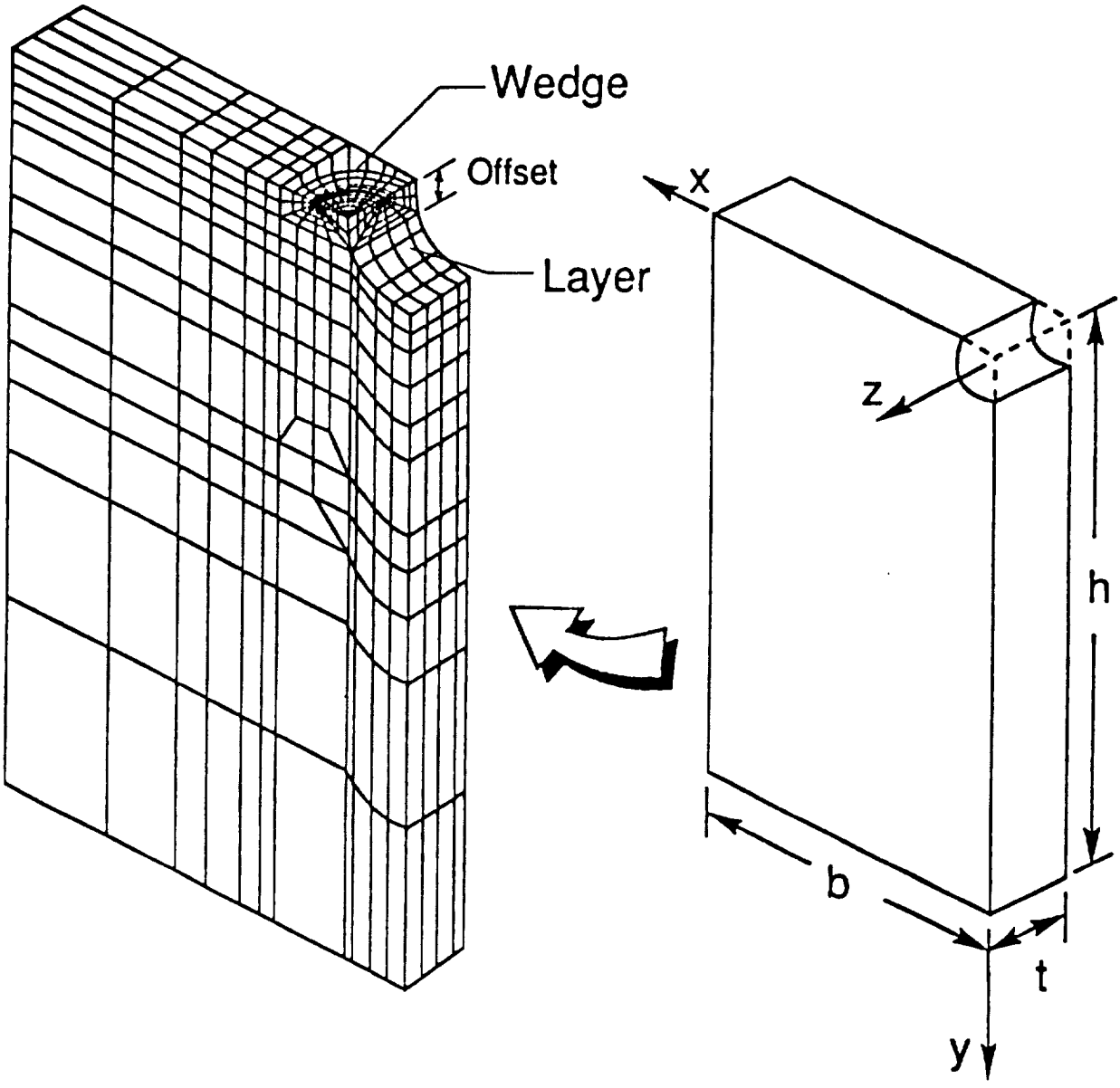

Figure 2. Typical finite-element model.

ORIGINAL PAGE IS
OF POOR QUALITY

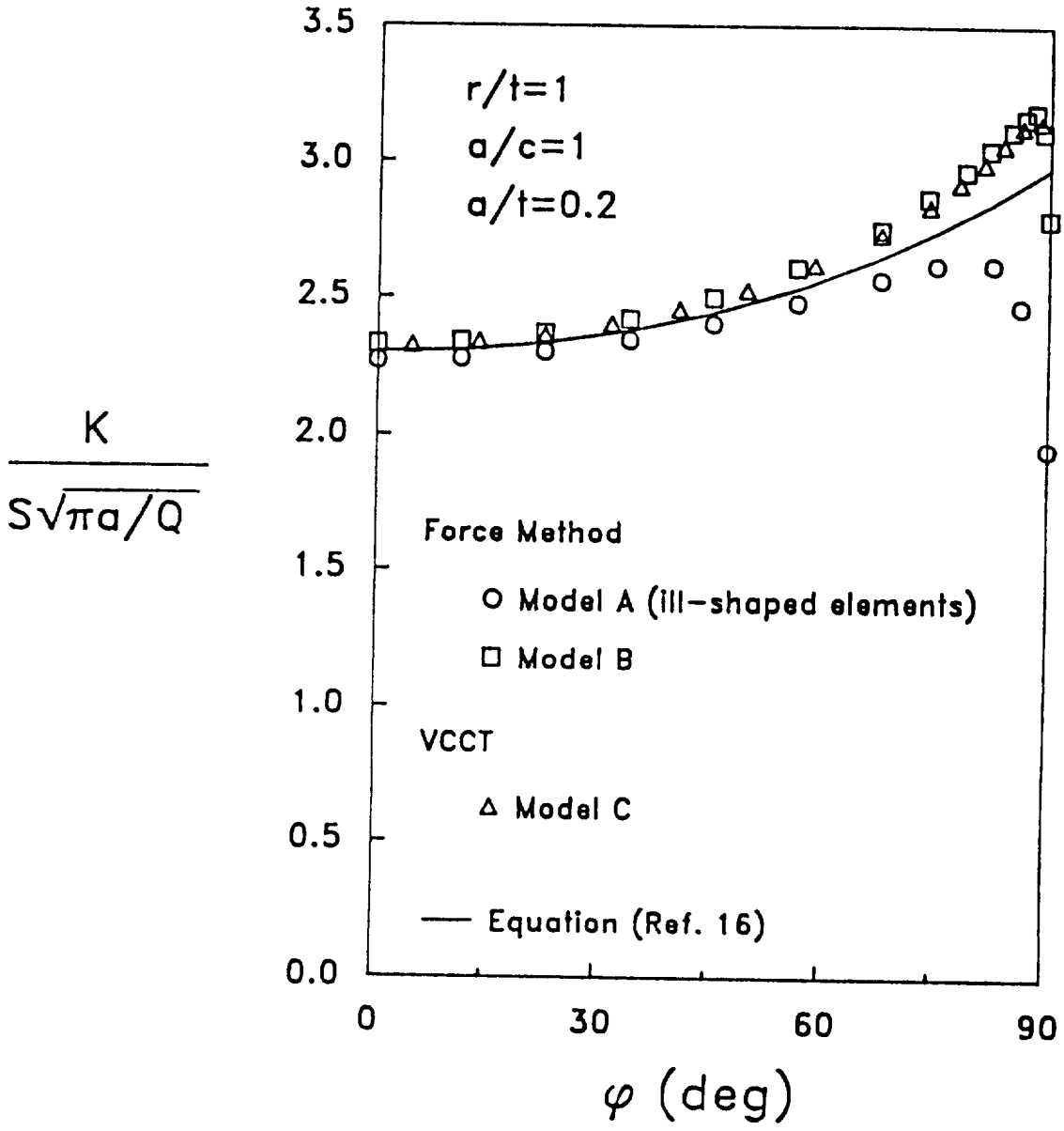

Figure 3. Comparison of results for a surface crack emanating from the center of a circular hole using various models and methods for r/t=1.

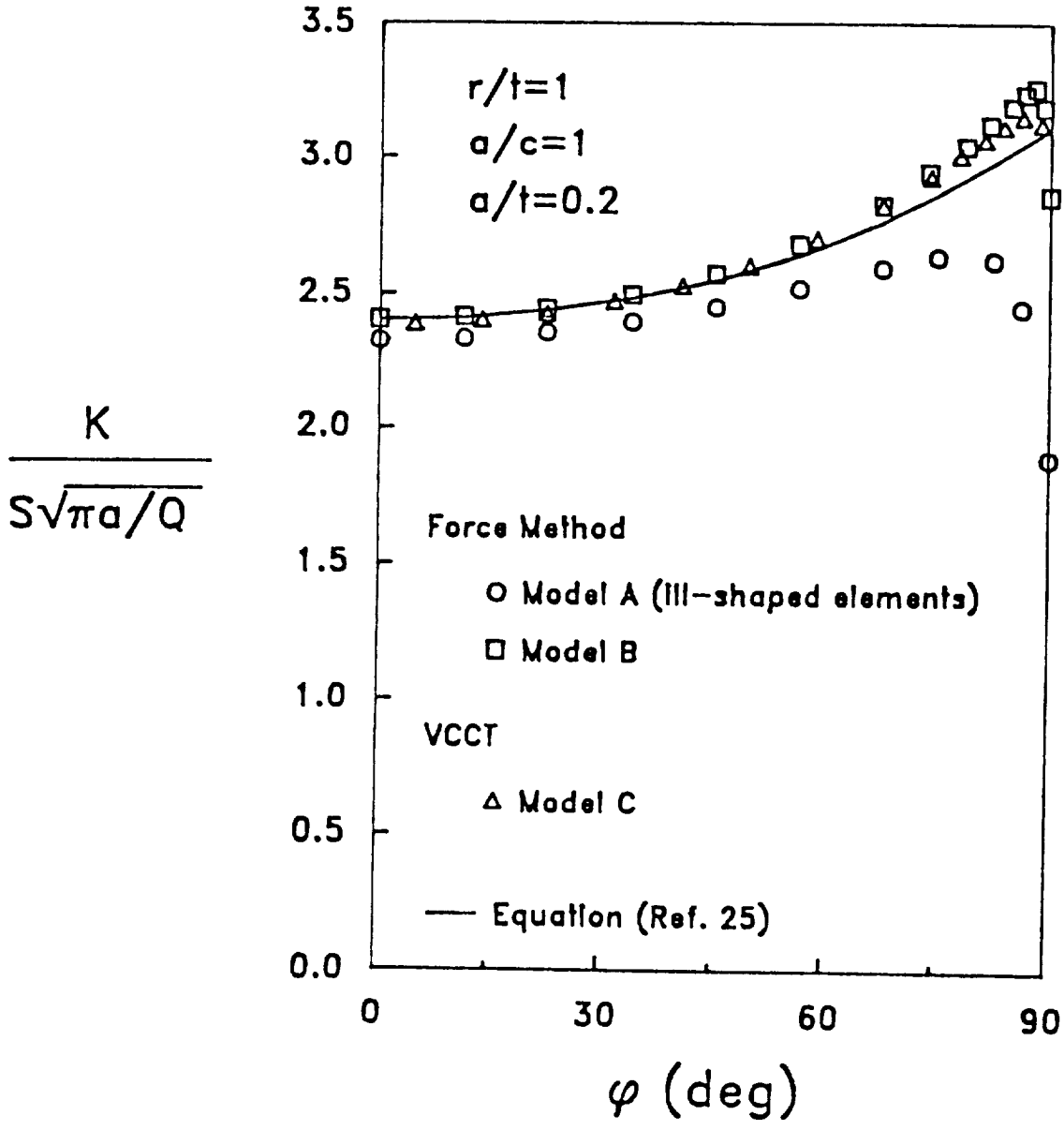

Figure 4. Comparison of results for a surface crack emanating from the center of a semi-circular notch using various models and methods for r/t=1.

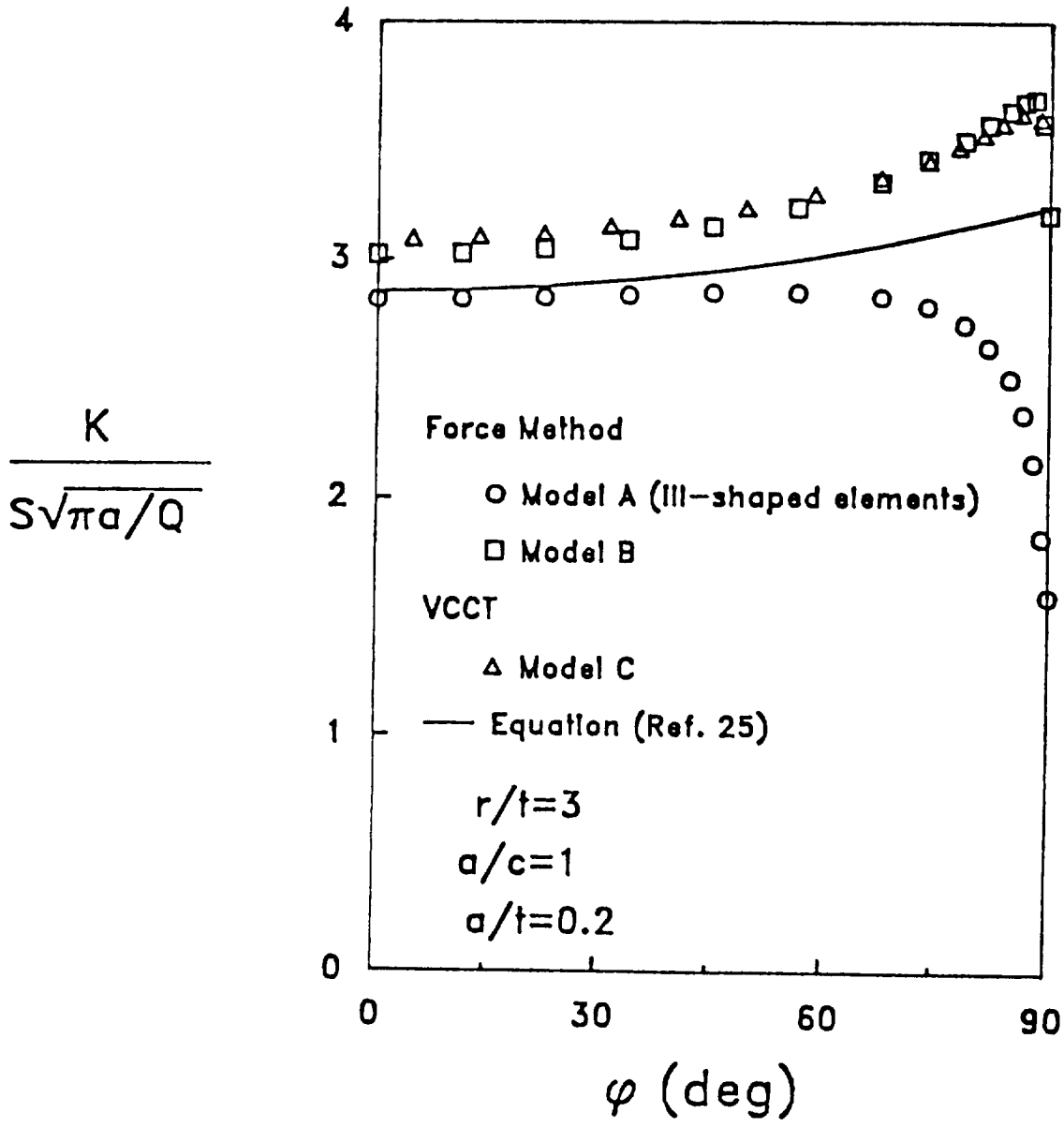

Figure 5. Comparison of results for a surface crack emanating from the center of a semi-circular notch using various models and methods for r/t=3.

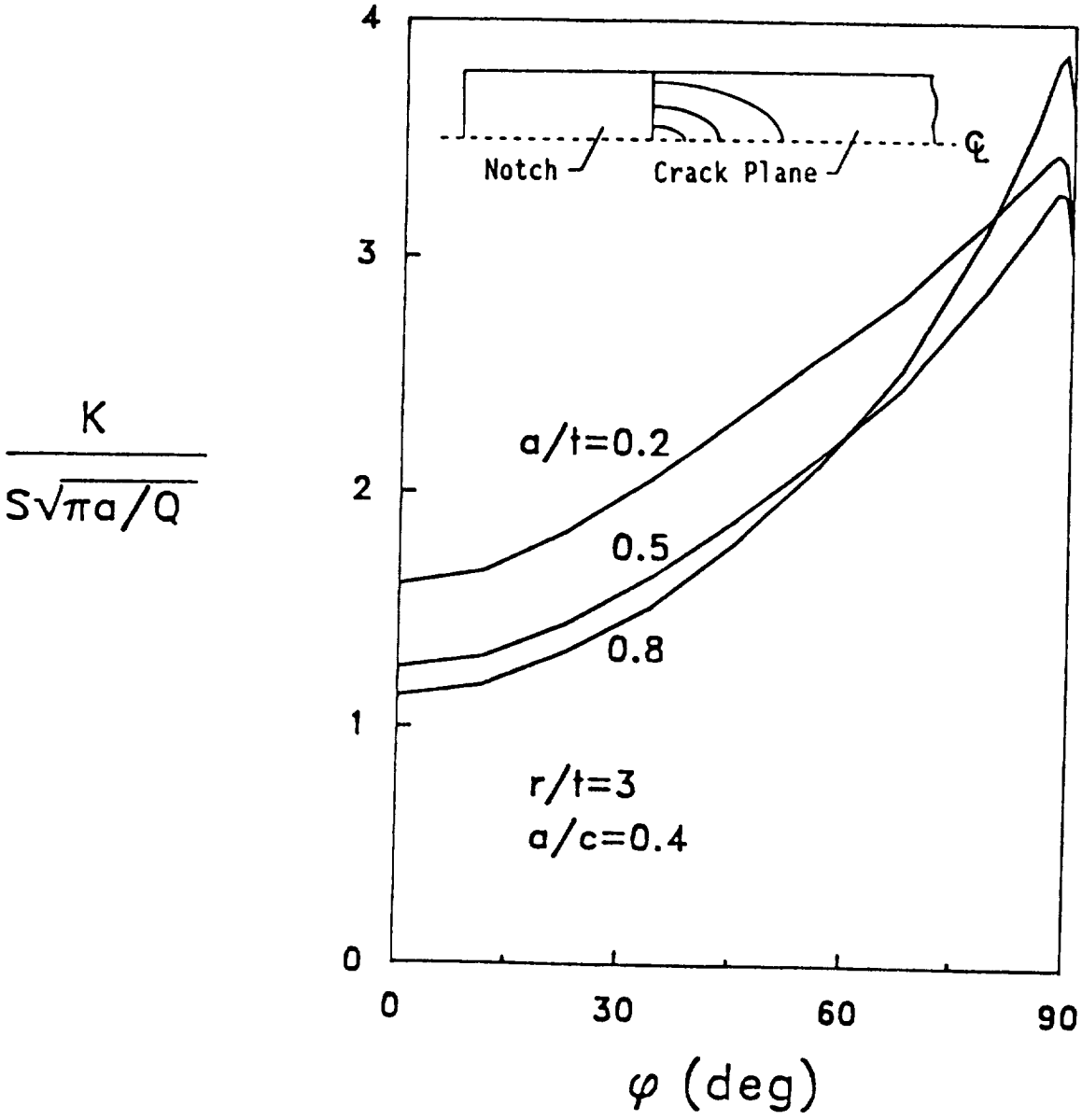

Figure 6. Boundary-correction factor distributions along crack front for semi-elliptical surface crack (a/c=0.4) at the center of the notch root.

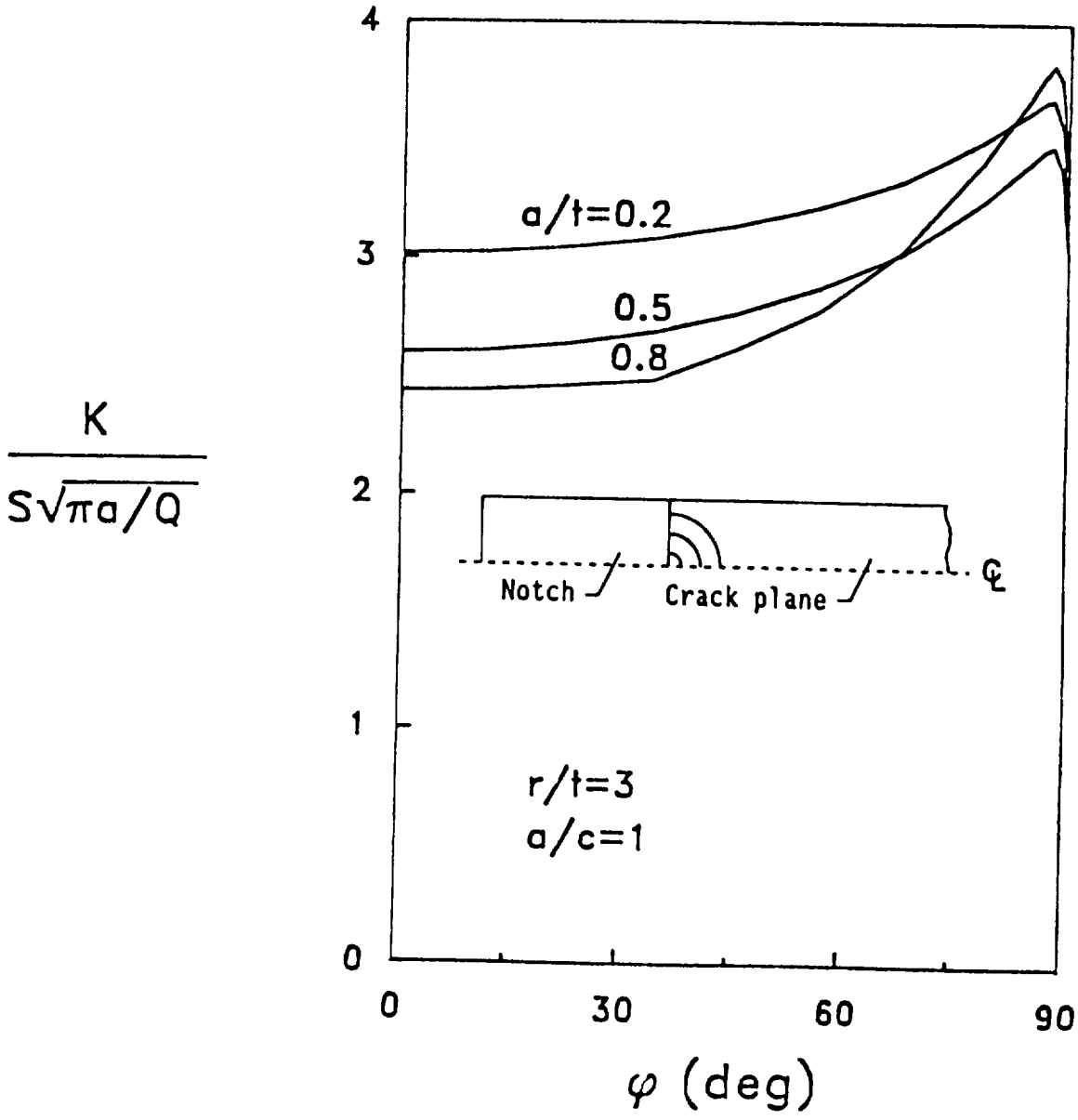

Figure 7. Boundary-correction factor distributions along crack front for semi-circular surface crack (a/c=1.0) at the center of the notch root.

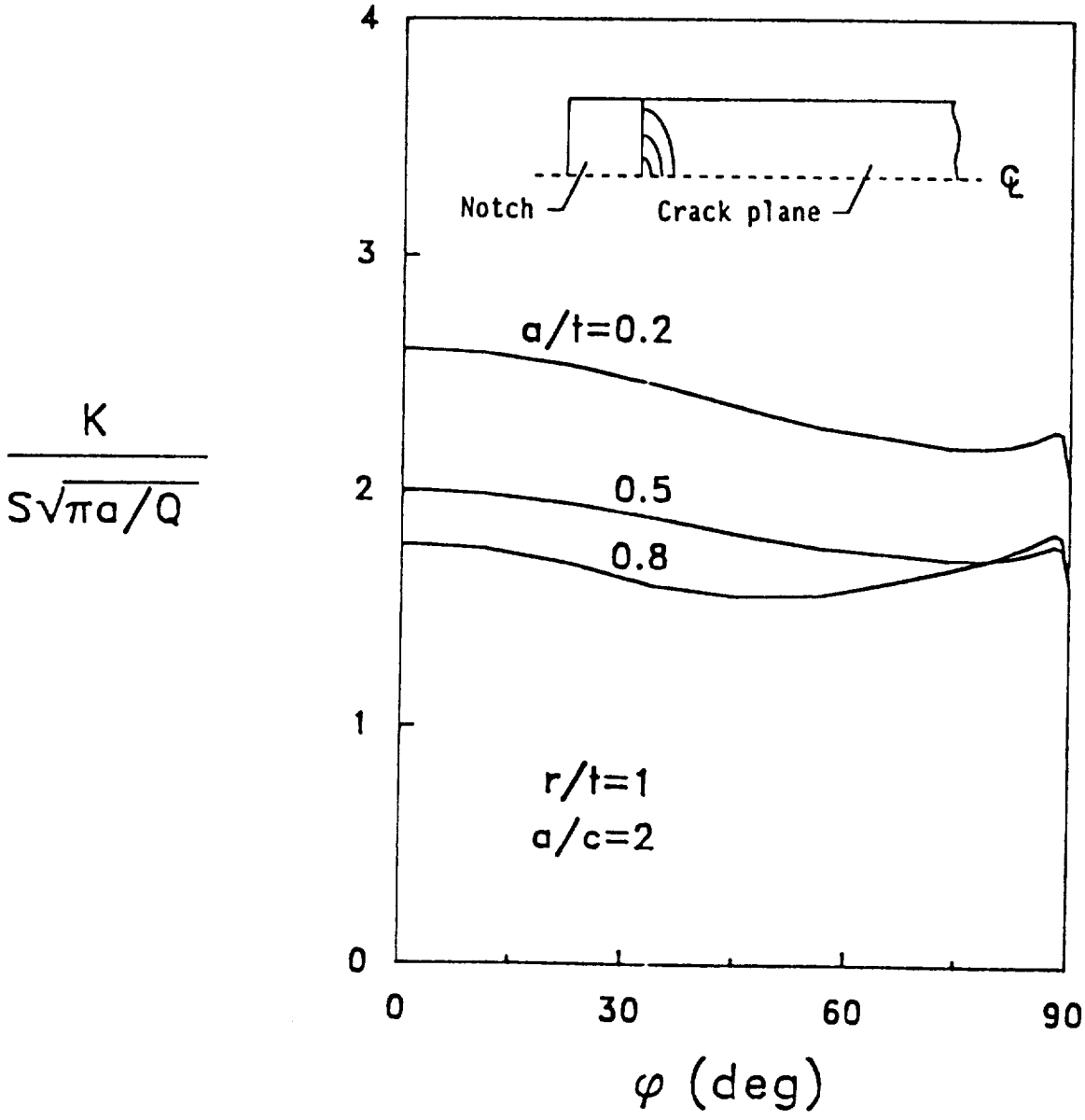

Figure 8. Boundary-correction factor distributions along crack front for semi-elliptical surface crack (a/c=2.0) at the center of the notch root.

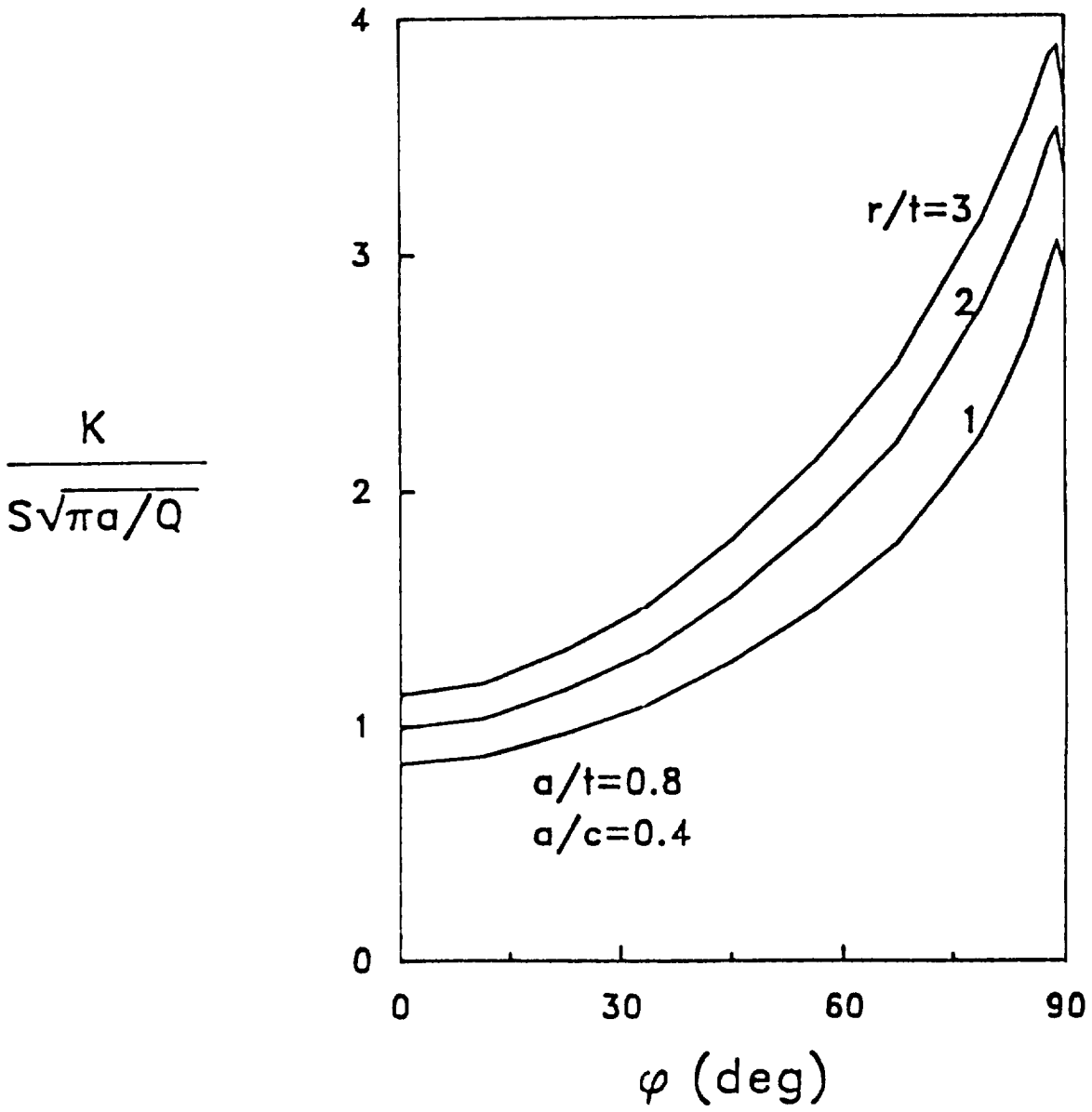

Figure 9. Effect of r/t on the distribution of boundary-correction factors for a deep semi-elliptical surface crack at the center of the notch root.

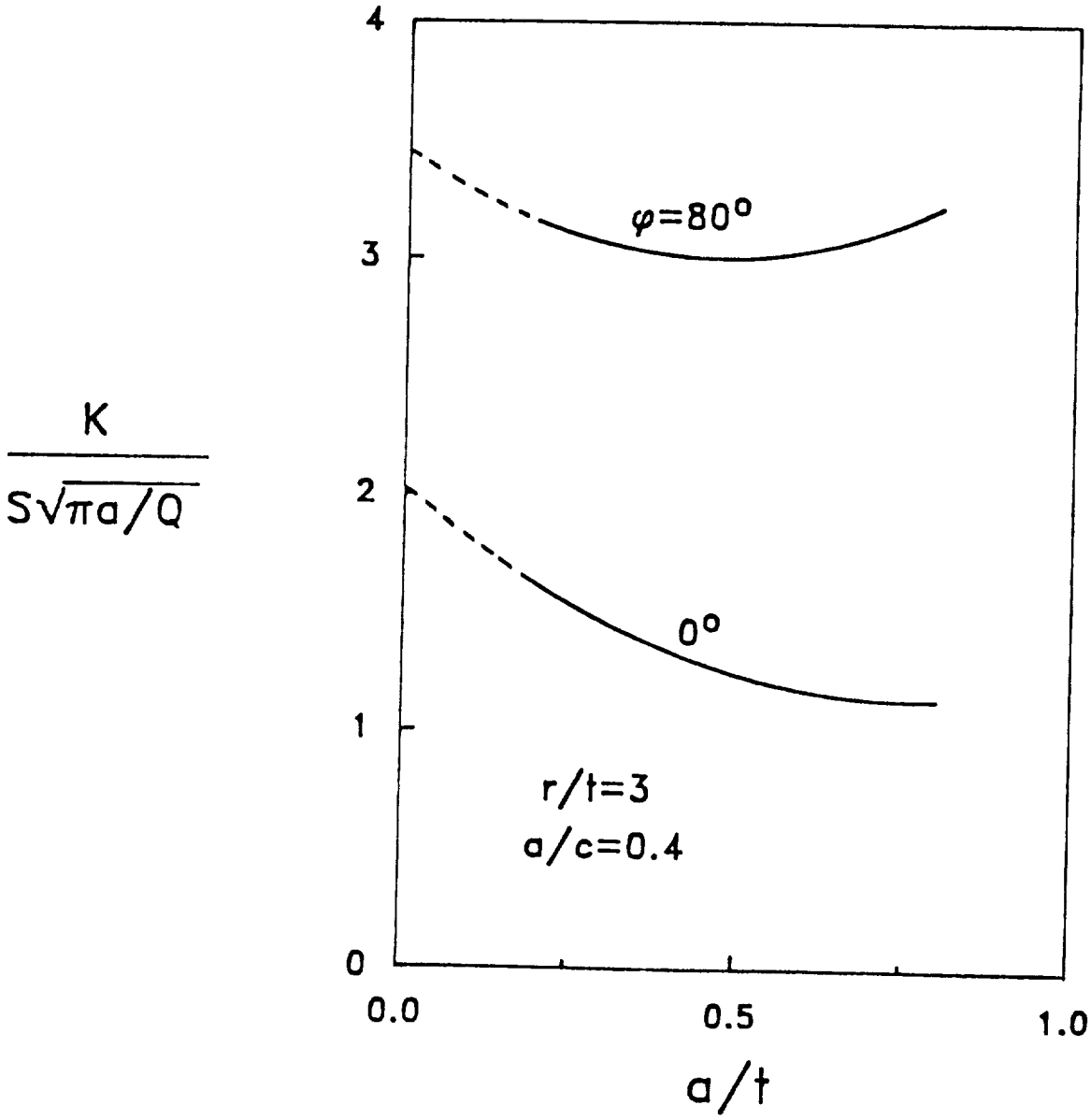

Figure 10. Effect of crack size on boundary-correction factors at the end of the major and near the end of the minor axes (ϕ=0° and 80°).

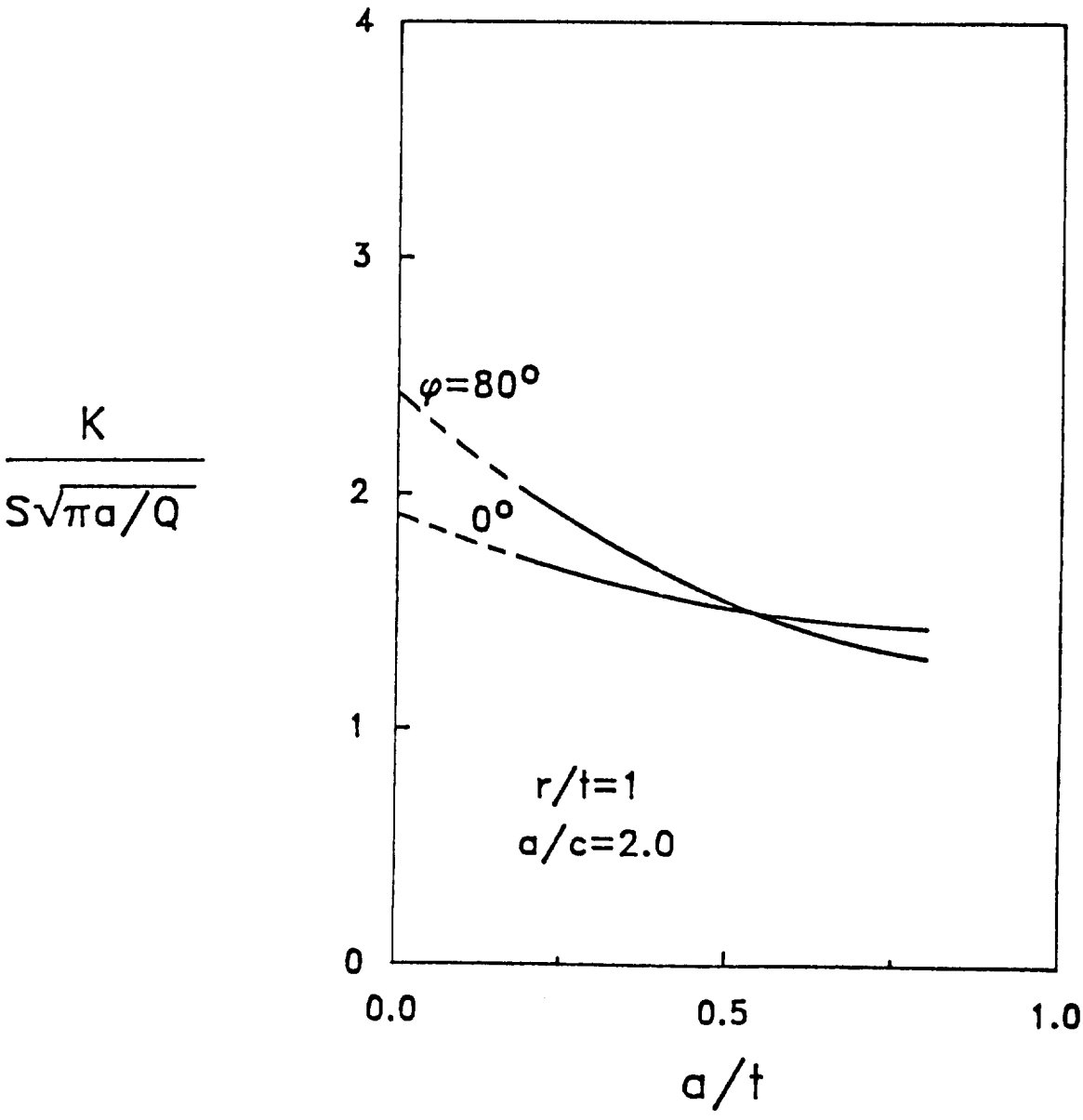

Figure 11. Effect of crack size on boundary-correction factors at the end of the major and near the end of the minor axes (ϕ=0° and 80°).

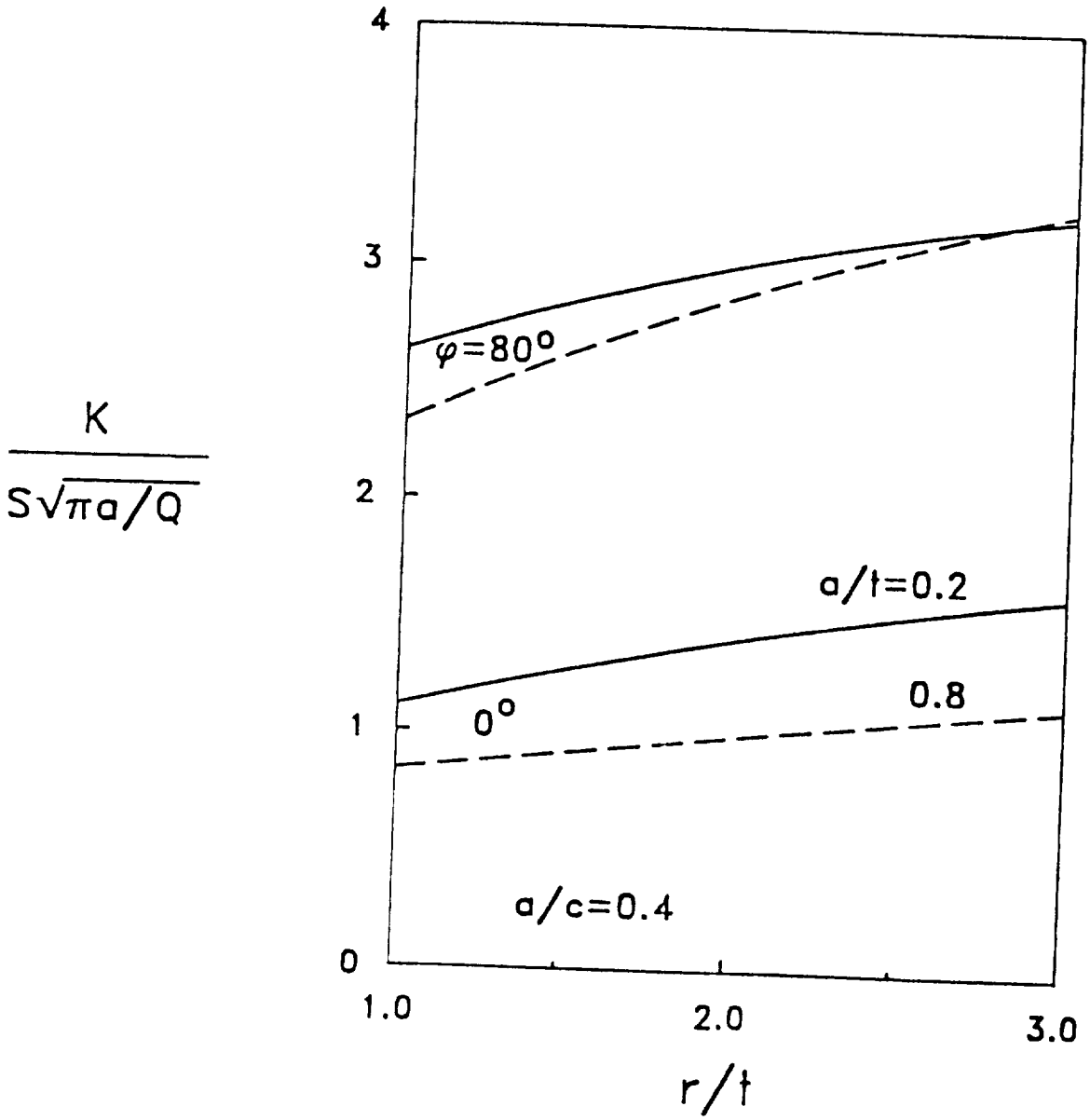

Figure 12. Effect of notch size on boundary-correction factors for a semi-elliptical surface crack at the end of the major and near the end of the minor axes (ϕ=0° and 80°).

NASA

Report Documentation Page

1. Report No.	2. Government Accession No.	3. Recipient's Catalog No.
NASA TM-101527		

4. Title and Subtitle

A Re-Evaluation of Finite-Element Models and Stress-Intensity Factors For Surface Cracks Emanating From Stress Concentrations

5. Report Date

November 1988

6. Performing Organization Code

7. Author(s)

P. W. Tan*, I. S. Raju*, K. N. Shivakumar*, and
J. C. Newman, Jr.

8. Performing Organization Report No.

10. Work Unit No.

505-63-01-05

9. Performing Organization Name and Address

NASA Langley Research Center
Hampton, VA 23665-5225

11. Contract or Grant No.

13. Type of Report and Period Covered

Technical Memorandum

12. Sponsoring Agency Name and Address

National Aeronautics and Space Administration
Washington, DC 20546

14. Sponsoring Agency Code

15. Supplementary Notes

*P.W. Tan; I.S. Raju; and K.N. Shivakumar, Analytical Services and Materials, Inc.
107 Research Drive, Hampton, VA 23666
J. C. Newman, Jr., Langley Research Center, Hampton, VA 23665-5225

16. Abstract

This paper presents a re-evaluation of the three-dimensional finite-element models and methods used to analyze surface cracks at stress concentrations. Previous finite-element models used by Raju and Newman for surface and corner cracks at holes were shown to have "ill-shaped" elements at the intersection of the hole and crack boundaries. These ill-shaped elements tended to make the model too stiff and, hence, gave lower stress-intensity factors near the hole-crack intersection than models without these elements. Improved models, without these ill-shaped elements, were developed for a surface crack at a circular hole and at a semi-circular edge notch. Stress-intensity factors were calculated by both the nodal-force and virtual-crack-closure methods. Both methods and different models gave essentially the same results. Comparisons made between the previously developed stress-intensity factor equations and the results from the improved models agreed well except for configurations with large notch-radii-to-plate-thickness ratios.

Stress-intensity factors for a semi-elliptical surface crack located at the center of a semi-circular edge notch in a plate subjected to remote tensile loadings were calculated using the improved models. The ratio of crack depth to crack length ranged from 0.4 to 2; the ratio of crack depth to plate thickness ranged from 0.2 to 0.8; and the ratio of notch radius to the plate thickness ranged from 1 to 3. The models had about 15,000 degrees-of-freedom. Stress-intensity factors were calculate by using the nodal-force method.

17. Key Words (Suggested by Author(s))	18. Distribution Statement
Cracks Surface cracks Crack propagation Fracture Stress analysis	Unclassified - Unlimited Subject Category - 39

19. Security Classif. (of this report)	20. Security Classif. (of this page)	21. No. of pages	22. Price
Unclassified	Unclassified	31	A03